SERS-Active Ag Nanoparticles on Porous Silicon and PDMS Substrates: A Comparative Study of Uniformity and Raman Efficiency

Chiara Novara,*[,†] Silvia Dalla Marta,[‡] Alessandro Virga,[†] Andrea Lamberti,[†] Angelo Angelini,[†] Alessandro Chiadò,[†] Paola Rivolo,[†] Francesco Geobaldo,[†] Valter Sergo,[‡] Alois Bonifacio,[‡] and Fabrizio Giorgis*[,†]

[†]Applied Science and Technology Department, Politecnico di Torino, Torino I-10129, Italy
[‡]Department of Engineering and Architecture, University of Trieste, Trieste I-34127, Italy

Supporting Information

ABSTRACT: Silver-coated porous silicon and polydimethylsiloxane (PDMS) are systematically analyzed as substrates for surface-enhanced Raman scattering (SERS). They were selected as representative metal−dielectric nanostructures characterized by different morphology and substrate dielectric constant which is reflected in the electromagnetic near-field intensity spectra. The study is conducted using 4-mercaptobenzoic acid as probe molecule with the aim to compare the scattering efficiency and the homogeneity of the Raman signal on the selected substrates. A larger SERS enhancement is evidenced for the silicon-based plasmonic nanostructures (>10^6, despite the electronic off-resonant excitation of the analyte). On the other hand, the silvered elastomeric substrates, characterized by a good Raman efficiency, show good repeatability featured by a low inter- and intrasubstrate standard deviation of the SERS signal intensity, which make them suitable for quantitative analysis. The influence of the excitation wavelength on such properties is deeply discussed taking into account experimental results and 3D modeling.

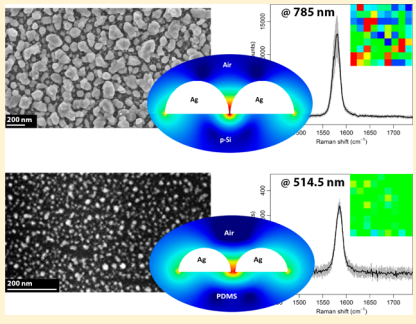

INTRODUCTION

Solid SERS (surface-enhanced Raman scattering) substrates show unique advantages over colloidal systems, such as stable aggregation state of metal nanoparticles (NPs) and easy integration in optofluidic devices.[1] The first issue is crucial, considering that the main contribution to the SERS effect is provided by the electromagnetic (EM) enhancement mechanism, in which the enhancement of the Raman scattering from molecules interacting with metallic NPs occurs through intense EM fields induced by the resonant excitation of localized surface plasmons (LSP).[2] Indeed, the EM enhancement is particularly sensitive to the spatial arrangement of the nanoparticles, as their optical properties are strongly dependent on interparticle interactions providing the well-known SERS hot-spots.[3] Furthermore, dielectric/semiconductive substrates hosting metallic nanostructures can be carefully selected in order to provide (i) additional Raman chemical enhancement through a charge transfer involving the electronic states of the analyte and of the substrate,[4] (ii) system flexibility, and/or (iii) high specific surface area.[5−7]

SERS substrates characterized by plasmonic NPs synthesized on either polymers or porous semiconductors have been the subject of previous studies and applications.[8−10] Among them, silver coated-porous silicon (Ag-pSi, produced by immersion plating of electrochemically etched silicon in silver nitrate solutions[11,12]) and polydimethylsiloxane (Ag-PDMS, produced by dc sputtering of silver NPs) were reported in the recent past as ultrasensitive SERS platforms. These metal−dielectric structures allow the detection of organic molecules at pico- and femtomolar concentrations (few/single molecule regime).[6,13]

In the framework of practical SERS applications in analytical and bioanalytical chemistry, it is worth to underline that the intrasubstrate uniformity and the intersubstrates repeatability of the detected signal intensity must be optimized, alongside with a high SERS efficiency.[14] The spatial inhomogeneity of the nanoparticles morphology and of the hot-spots distribution are the main reasons of fluctuations in SERS intensity.[15] Following the recent literature, relative standard deviations (RSDs) of the SERS signal intensity close to 20% are usually considered a good result.[16−18] However, the attainment of substrates, characterized by smaller RSD values than 10%, required for quantitative analysis, is still a very challenging target.[19]

In this study, we critically compare the performance of Ag-pSi and Ag-PDMS SERS substrates, which represent classes of nanostructures whose SERS response is determined by the merging of the different morphologies and substrate dielectric constants, in view of reliable applications. SERS substrates are characterized in terms of uniformity and efficiency by statistical analysis of the spectra extracted from the SERS maps of a

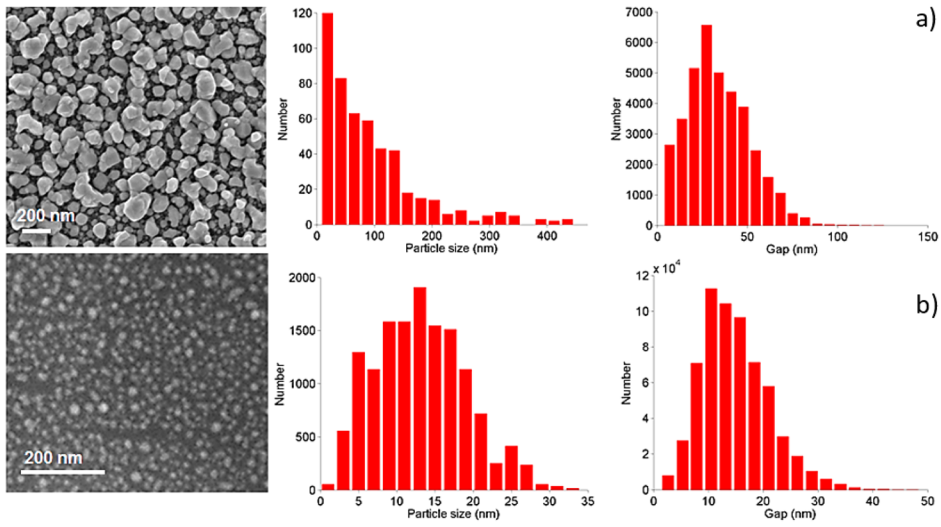

Figure 1. FESEM micrographs of the silver nanoparticles, the corresponding distributions of particle size, expressed as equivalent diameters, and the interparticle gap distributions obtained by image analysis for optimized (a) porous silicon and (b) PDMS substrates.

nonresonant analyte, 4-mercaptobenzoic acid (4-MBA), employing several excitation wavelengths (514.5, 632.8, and 785 nm). New insights into the plasmonic properties of the nanostructures are also provided by 3D finite element modeling, thus corroborating the experimental findings.

EXPERIMENTAL DETAILS, DATA ANALYSIS, AND MODELING

Materials. *SERS Substrates Fabrication.* Porous silicon (pSi) was prepared starting from a highly boron doped silicon wafer (34−40 mΩ·cm resistivity) by etching in a 20:20:60 HF:H_2O:CH_3CH_2OH solution for 30 s with a current density of 125 mA/cm^2. The so-prepared layers showed a porosity of 64% and a thickness of 1950 nm. Samples were then immersed in aqueous $AgNO_3$ (10^{-2} M) for 60 s at 50 °C to synthesize silver NPs. An annealing at 500 °C for 5 min was performed before SERS measurements in order to clean the silver surface from any contaminant.

PDMS slices were prepared by mixing the prepolymer and the curing agent (Sylgard 184, Dow Corning) with a 20:1 weight ratio, degassing for 1 h, casting the mixture into a PMMA mold (fabricated by a milling machine), curing in a convection oven for 1 h at 70 °C, and finally manually peeling off the self-standing membranes. Ag NPs were deposited on the PDMS membranes by dc sputtering in Ar atmosphere (Q150T-ES, Quorun Technologies) using a sputtering current of 40 mA for 5 s; the PDMS membranes were at 5 cm from the Ag target.

4-MBA Incubation Protocol. 4-MBA (Sigma-Aldrich) was dissolved in methanol at 10^{-3} M concentration. Aqueous 4-MBA solutions were prepared by dilution in water (in the range 10^{-4}−10^{-8} M) and used to incubate the SERS substrates for 5 min. The samples were gently rinsed with water after the incubation.

Characterizations. Scanning electron microscopy images of silvered samples were obtained as secondary electron contrast images with 5 keV (Ag-pSi) and 10 keV (Ag-PDMS) electrons using an in-lens detector of a Zeiss SUPRA 40 (Zeiss SMT, Oberkochen, Germany) field emission electron microscope (FESEM).

Specular reflection or transmission spectra were acquired using an Agilent Cary 5000 (Agilent, Santa Clara, CA) UV−vis−NIR spectrophotometer equipped with a 12.5° reflectance unit in the 200−1000 nm range.

SERS spectra of 4-MBA were obtained by means of a Renishaw inVia Reflex micro-Raman spectrophotometer (Renishaw plc, Wotton-under-Edge, UK) equipped with a cooled CCD camera. Three laser sources were used to excite the samples: a 785 nm diode laser (Toptica, with a 450 mW output power), a 632.8 nm HeNe laser (Melles-Griot, 35 mW), and a 514.5 nm Ar-ion laser (Modulaser, 50 mW). Raman/SERS imaging was performed on four substrates for each typology and wavelength. The maps were acquired with a 10× objective on a 400 μm × 400 μm area with a 50 μm step.

Filters were used to reduce the laser power at the sample in order to avoid thermal and photodegradation. In particular, 1% of the laser output power was used for maps at 785 nm excitation; either 50% and 100% of the output power was used at 632.8 nm excitation, depending on the substrate type (Ag-pSi or Ag-PDMS); finally, 100% of the laser output power was used at 514.5 nm. Furthermore, defocusing of the laser spot on the sample was applied (70%, 80%, and 90% at 514.3, 632.8, and 785 nm, respectively) to keep the laser power density low enough in order to avoid analyte degradation.

SERS data were preprocessed and analyzed using the *hyperSpec* package[20] in R.[21]

SEM Image Analysis and FEM Modeling. Ag particles diameter and interparticle gap distributions were extracted by FESEM images by applying a homemade MATLAB algorithm on an area of 10 μm^2 (images with ×200 000 magnification). In detail, each nanoparticle was approximated by a circular "equivalent particle" having the same planar area, obtaining the diameter distributions. The distributions of the gap between neighboring nanoparticles were obtained by applying the distance transform function to the FESEM images, a MATLAB operator that replaces each background pixel value with the distance from the closest NP, by considering the local maxima of the obtained map as the half gap value at each point.

The near-field EM intensity spectra within the nanogap of dimers of Ag hemispheres, which lie on porous silicon and PDMS substrates, were modeled by COMSOL Multiphysics software (3D Finite Element Method). Several hemisphere diameters, interparticle gaps, and the dielectric constant dispersion of the two dielectric substrates were considered.

For the porous silicon substrates, the optical dispersion has been extracted by spectral reflectance measurements performed on bare electrochemically etched silicon layers. The formation of Si oxide on the surface of the thermally treated substrate was neglected, as the decrease of the calculated refractive index was verified to be lower than 10% compared to the nonoxidized Si.

RESULTS AND DISCUSSION

Morphology and Optical Analysis of Ag-Coated pSi and PDMS. The Ag-pSi substrates were synthesized by immersion of porous silicon layers (average pore dimension ∼2−20 nm, as shown in the FESEM top view of Figure S1) in an $AgNO_3$ aqueous solution as detailed in the previous section. A redox process involving the reduction of Ag^+ cations by the hydrides covering the pSi surface promotes the synthesis of Ag NPs.[22] On the other hand, Ag-PDMS substrates were synthesized manufacturing the elastomeric slabs with standard replica molding procedures, with a successive growth of Ag particles by dc sputtering in an Ar atmosphere.

The FESEM micrographs, reported in Figure 1, evidence a noticeable morphological difference between the two substrate typologies. The Ag-pSi samples show a polydispersion of the Ag NPs characterized by an average size of ∼100 nm with a relative standard deviation (RSD) = 85%; the average interparticle gap is ∼25 nm with a RSD = 48%. A wide range of particle sizes (5−400 nm) is observed, as shown by the histogram distributions in Figure 1a. Such a large dispersion can be justified by taking into account the growth mechanism: after the first nucleation steps most of the Ag particles increase their size, after which new populations with small size appear within the interstices between larger particles. The Ag-PDMS substrates present a polydispersion of the Ag NPs with an average size of ∼12 nm with a RSD = 46% and an average interparticle gap of ∼15 nm with a RSD = 41% (Figure 1b). In this case, the narrower dispersions can be ascribed to the sputtering growth kinetics, where the NPs size is limited by the short deposition time employed to avoid the formation of a homogeneous silver thin film. Despite the highlighted differences, both types of substrates show a certain fraction of nanometer interparticle gap sizes, which can yield the coupling of gap plasmons (and thus the presence of hot spots) under light excitation.[23] In particular, cross-sectional FESEM micrographs of Ag-pSi evidence the presence of very small gaps of a few nanometers (Figure S2a).

In the past, the optical response of the discussed metal−dielectric nanostructures has been analyzed by transmission and/or reflectance spectroscopies, where the spectral dips were identified as plasmon resonances, which give rise to enhanced absorption/scattering processes.[6,12,13] Such dips were considered optical fingerprints for the suitable choice of the SERS substrate vs a specific excitation energy. Actually, the higher signal enhancements are obtained when the wavelength of a LSP resonance of the nanostructure is close to the excitation wavelength or, more exactly, when such resonance is between the excitation and the Raman emission wavelengths.[24]

The measurements reported in Figure 2 show that the Ag-pSi and Ag-PDMS nanostructures share similar optical features, characterized by a plasmonic dip around 500 nm. As expected, the spectral width is broader for the Ag-pSi substrates, as it represents the convolution of different LSP resonances of nanostructures characterized by a larger distribution of particle diameters and interparticle gap sizes. Note that UV−vis reflectance/transmission spectra only provide information on

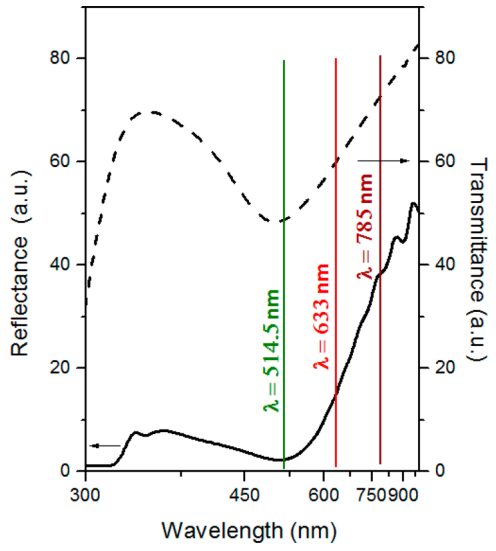

Figure 2. Typical specular reflectance spectrum of Ag-pSi (solid line) and transmission spectrum of Ag-PDMS (dashed lines) samples shown in Figure 1a,b. Vertical lines mark the excitation wavelengths employed in this study.

propagating scattered light, as they are insensitive to many EM near-field modes which can be effective in the Raman excitation. In order to give a first insight about the near-field modes of the discussed nanostructures, 3D finite element simulations were performed by considering a simple model, which consists in dimers of Ag hemispheres deposited on pSi and PDMS substrates (see Figure S3a,b). In particular, the contribution of the semiconductive and elastomeric matrixes is taken into account by using the dispersion of the dielectric functions of porous silicon and PDMS lying beneath the Ag hemispheres. The hemispherical shape can be inferred by the FESEM cross-sectional micrographs (Figures S2a and S2b for Ag-pSi and Ag-PDMS, respectively), in agreement with previous literature findings.[25] Figure 3 shows the calculated EM near-field intensity spectra within the dimer nanogaps, considering several hemisphere diameters and interparticle gap sizes. Both substrate types feature multiple resonances, covering the blue-green energy range for the PDMS-based structures and the visible−NIR energy range for the pSi-based ones. Independently from the material that underlies the Ag particles, the resonance occurring at the higher wavelength is subjected to a blue-shift and to an intensity quenching by increasing the interparticle gap, so reaching an asymptotic energy value when the gap goes beyond the hemisphere diameter. Moreover, by fixing the geometrical dimer parameters, a red-shift of the main resonance can be observed by increasing the substrate dielectric constant (see Figure 3a), consistently with past literature.[26,27]

The discussed dimer model represents an extreme simplification when compared to the complex morphology of the real nanostructures. Nevertheless, some hypotheses can be put forward regarding the dependence of their SERS efficiency on the excitation wavelength. Indeed, a noticeable SERS effect can be expected for Ag-pSi substrates in both the visible and red-NIR range. For Ag-PDMS specimens, a good SERS efficiency is expected around 500 nm, with a weakening when the excitation wavelength is red-shifted.

SERS of Mercaptobenzoic Acid. SERS efficiency and uniformity of the samples are determined at three commonly used laser excitation energies by using 4-MBA as probe analyte.

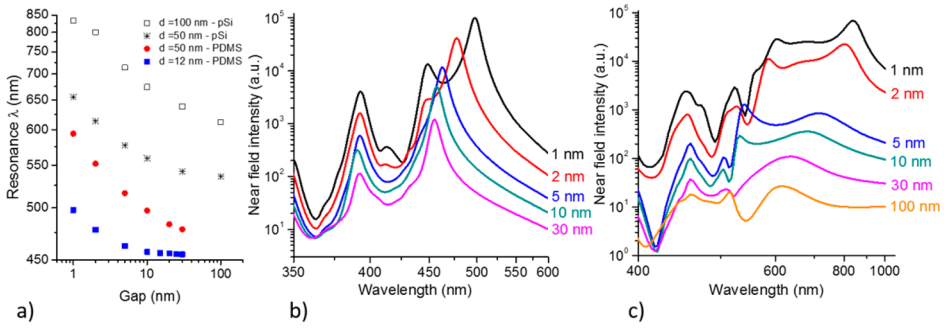

Figure 3. (a) Resonance wavelength of the lowest energy mode versus the dimer interparticle spacing. The resonance wavelength is extracted from the modeled EM near field intensity spectra for a dimer of Ag hemispheres supported on pSi (sphere diameter d = 50 and 100 nm) and PDMS (sphere diameter d = 12 and 50 nm). Spectra were calculated within the nanogap. Selected spectra at representative d = 12 nm for Ag-PDMS (b) and d = 100 nm for Ag-pSi (c) are shown for different nanogap sizes.

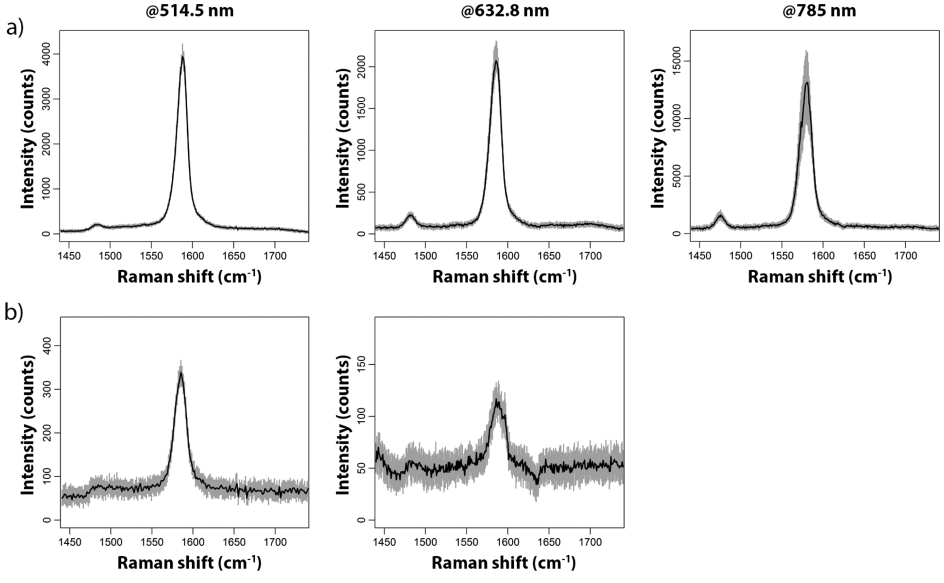

Figure 4. Average SERS spectra of 10^{-5} M 4-MBA calculated from the Raman maps acquired at 514.5, 632.8, and 785 nm on (a) Ag-pSi and (b) Ag-PDMS. Shaded areas represent interquartile range (first−third quartile) of the collected data. No 4-MBA spectral signature could be detected at 785 nm on Ag-PDMS substrates, and therefore data are not reported.

Thanks to its electronic off-resonant behavior in the covered wavelength range,[28] such molecule is particularly suitable for multiwavelength studies because the observed SERS intensity only depends on the plasmonic features of the SERS substrate and not on the possible electronic resonances of the probe. Moreover, a uniform distribution of the analyte on the SERS substrate surface is expected due to the incubation followed by the rinsing step, which is enabled by the efficient bonding of 4-MBA to the silver surface through its thiol group. Raman mapping of several replicas of Ag-pSi and Ag-PDMS substrates is performed after samples incubation in aqueous 4-MBA solutions at 10^{-5} M concentration (as detailed in the Experimental Details section).

Spectra averaged over the entire map area, along with the first and third quartile of the data distribution, highlighted as shaded area, are shown in Figure 4a,b for Ag-pSi and Ag-PDMS at 514.5, 632.8, and 785 nm. The typical features of 4-MBA, such as the intense 1584 cm^{-1} ring breathing mode and the broad 1380 cm^{-1} band attributed to the COO^- stretching,[29] are clearly observed (a wider range spectrum and bands assignments can be found in the Supporting Information, Figure S4 and Table S1).

Figure 5 shows the SERS maps of representative Ag-pSi and Ag-PDMS substrates collected at the excitation wavelengths which yield the highest intensity (785 and 514.5 nm for Ag-pSi and Ag-PDMS, respectively); the integrated intensity over the area of the band centered at 1584 cm^{-1} is depicted. First, all the collected spectra were normalized to the intensity of the TO-LO Raman peak of a c-Si layer (520 cm^{-1}) in order to obtain a reliable comparison at the different laser wavelengths. The average values of the 1584 cm^{-1} band intensities for each map were then reciprocally normalized in order to qualitatively convey the information about the heterogeneity of the SERS signal throughout the surface of the substrate and thus about the intrasubstrate repeatability of collected spectra.

Very different responses of SERS signal intensity to changes of the excitation energy are observed for the Ag-pSi and Ag-PDMS substrates. Figure 6 shows the dispersion of the SERS intensity (1584 cm^{-1} 4-MBA band) for different replicas of the same substrate types. It is worth to notice that a SERS mapping analysis of the substrates yields a distribution of intensities which is normal (Gaussian) only for the Ag-PDMS samples (as verified by the Shapiro−Wilk test performed on all the substrates; see Figure S5). Thus, the results are compared in

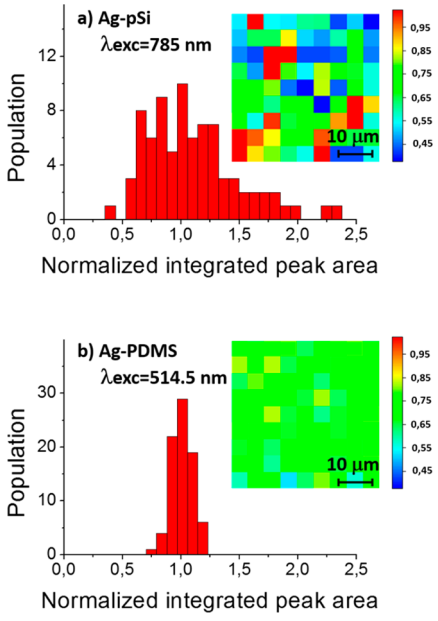

Figure 5. SERS maps and relative intensity distributions of representative substrates coated with 4-MBA. The diagrams plot the area of 4-MBA Raman peak at around 1584 cm^{-1}. In all the histograms the intensities were normalized with respect to the average SERS intensity.

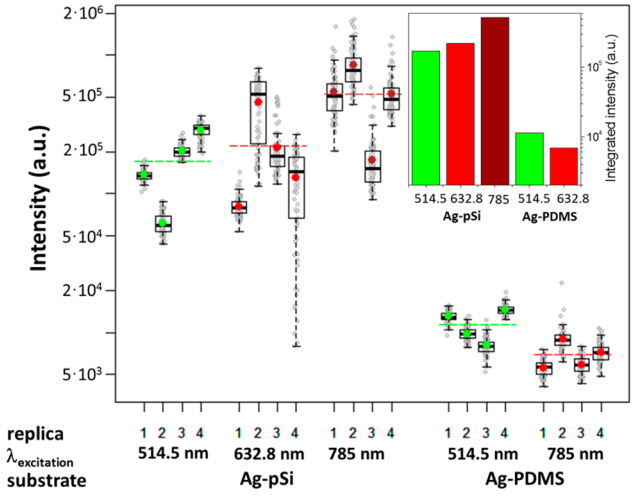

Figure 6. Comparison of the SERS intensities of the 4-MBA peak at around 1584 cm^{-1} (band area) collected by the SERS mapping for Ag-pSi and Ag-PDMS substrates, excited at 514.5, 632.8, and 785 nm. Four replicas were analyzed for each substrate type. The bottom and the top of the box (Tukey's plot) are the first and the third quartiles of the data distributions, the bands inside the box are the second quartiles (medians), the filled symbols represent the mean values, and the horizontal dashed lines show the average values for each replica set. The whiskers represent the 1.5-fold interquartile range. The inset shows the histogram plot of the averaged SERS intensities.

a Tukey's box plot, where the SERS intensity data are depicted through their median and quartiles values. In particular, the inset of Figure 6 shows the histogram representation of the average SERS intensity for the two substrates at the three excitation wavelengths. Ag-PDMS exhibits the highest SERS intensity for an excitation at 514.5 nm. The intensity decreases exciting the system at the longer wavelengths, where 4-MBA 10^{-5} M concentration cannot be detected for excitation at 785 nm.

On the other hand, the excitation profile of the Ag-pSi substrates shows an increase in SERS intensity going from 514.5 to 785 nm. This behavior is not predictable from the analysis of Ag-pSi UV−vis reflectance spectra, where the wide plasmonic dip is centered around 500 nm and no feature can be singled out in the NIR range (with the exception of the Fabry−Perot interference fringes due to the finite thickness of the pSi layer). However, as stated before, the reflectance spectra can typically detect far-field EM processes, while the near-field modes evidenced by the FEM modeling in terms of intense long-wavelength resonances in the range of 700−850 nm could be responsible of this experimental finding. As an example of nonradiating modes, the recent literature analyzed the dark plasmons, detected in different nanogaps and aggregated nanostructures[30,31] and potentially responsible for huge Raman signal enhancements.[32]

Moreover, Figure 6 shows as 4-MBA, adsorbed on the Ag-pSi substrates, provides a higher SERS intensity in comparison to the same analyte on Ag-PDMS ones for all the excitation wavelengths. Such behavior can be justified by considering the multiple resonances evidenced by the modeled EM near-field spectra. Indeed, the EM field localization can be markedly stronger by increasing the dielectric function of the material due to plasmon coupling to the metal nanoparticle at the interface with dielectrics, as discussed in previous studies.[33,34]

Uniformity of SERS Substrates. The intra- and intersubstrate fluctuation of the Raman signal intensity (4-MBA band at 1584 cm^{-1}) was carefully calculated and analyzed on the basis of the above-mentioned SERS mapping measurements. Table 1 summarizes the obtained values concerning substrate uniformity and reproducibility. A low variability is observed for Ag-PDMS substrates. Standard deviations around 10% and 20% are found for excitation at 514.5 nm for the intra- and intersubstrate analysis respectively, thus suggesting that the Ag-PDMS is a better SERS substrate than the Ag-pSi for the quantitative analysis. Despite the large Raman signal intensity provided by the Ag-pSi samples (see Figure 6), the intra-substrate intensity fluctuation is acceptable at 514.5 nm only, as it increases dramatically for excitation at higher wavelengths, while the intersubstrate SERS intensity fluctuation is rather large for all the excitation wavelengths. By taking into account the discussed FEM modeling, which assigns LSP resonances in the range of 630−800 nm to small interparticle gaps, the increase of the Raman intensity RSD upon excitation at 632.8 nm/785 nm could be explained by the sparse dispersion of the Raman hot-spots (lying in the nanosized Ag interparticle gaps) responsible for the SERS enhancement at such wavelength. Actually, a low concentration of small interparticle gaps can be expected within the microsized exciting laser spot, leading to low signal averaging. Moreover, the enhancement provided by the hot-spots is very sensitive to the local environment, which can strongly differ from one hot-spot to another,[35,36] as it depends on the gap geometry. The combined efficiency and uniformity analysis clearly shows that the Ag-pSi samples are characterized by a large efficiency, especially at 785 nm, and therefore they are good and versatile SERS substrates for qualitative analysis, but not for quantitation, as better clarified in the next section.

MBA SERS Spectra at Different Concentrations. In light of the discussed results, the external amplified Raman efficiency (EARE)[37] of the substrates has been calculated for Ag-PDMS

Table 1. Summary Statistics for SERS Mapping of Four Replicas Concerning the Ag-Coated Porous Silicon (Ag-PSi) and PDMS (Ag-PDMS) Substrates for All the Used Excitation Wavelengths

substrate	excitation (nm)	replica	intrasample IQR/median[a] (%)	intrasample RSD[b] (%)	RSD of intensity averages[d] (%)
Ag-pSi	514.5	1	10.2	9.3	48.4
		2	25.5	17.1[c]	
		3	13.1	10.3	
		4	15.4	12.8[c]	
	632.8	1	18.2	17.1	65.4
		2	78.9	46.5[c]	
		3	34.1	44.1[c]	
		4	81.8	53.7[c]	
	785	1	45.3	40.8[c]	45.3
		2	39.7	35.9[c]	
		3	53.8	48.3[c]	
		4	35.6	34.5[c]	
Ag-PDMS	514.5	1	11.3	9.1	22.7
		2	14.0	10.9	
		3	16.1	15.2	
		4	10.2	9.0	
	632.8	1	18.8	13.8	19.7
		2	16.6	22.2	
		3	20.8	13.8	
		4	21.2	17.5	

[a]Interquartile range of the integrated intensity ot the 4-MBA Raman band centered at 1584 cm^{-1} normalized to the median value for each map (representative of intrasample variability). [b]Relative standard deviation of the integrated intensity (within one map). [c]RSD as an indicator for data variability for non-normal distributions should be taken with caution. [d]Relative standard deviation of the integrated intensity averages calculated for each map (representative of intersample variability).

(excitation at 514.5 nm) and for Ag-pSi (excitation at 514.5 and 785 nm) substrates. The EARE represents a parameter that estimates the enhancement ability of SERS substrates when their complex morphology makes hard to define the actual adsorbed amount of molecules, hence complicating the rigorous Raman enhancement factor. This value is calculated as the ratio between the minimum analyte concentration detectable on the bare support (pSi or PDMS) and the minimum concentration detected on the sample coated by plasmonic nanoparticles (Ag-pSi or Ag-PDMS substrate). In order to determine the EARE, Ag-coated samples and noncoated counterparts are incubated in 4-MBA solutions at increasing concentrations (10^{-8}–10^{-4} M for the Ag-coated substrates and up to 10^{-1} M for the bare support). The related data, presented in Figure 7, show the 1584 cm^{-1} band intensity as a function of the analyte concentration, besides the experimentally acquired 4-MBA SERS spectra, for the silvered samples.

Upon 514.5 nm excitation, 4-MBA can be detected at a molar concentration as low as 10^{-7} M on Ag-PDMS and at 5×10^{-8} M for Ag-pSi. As the analyte is not detectable on the bare substrates until 10^{-1} M concentration, an EARE of 10^6 and 2×10^6 can be calculated for Ag-PDMS and Ag-pSi, respectively (see the details in section 5 and Table S2 of the Supporting Information). Such enhancements are relevant considering the nonresonant behavior of 4-MBA in the visible range. Concerning the excitation at 785 nm, 4-MBA can be detected on Ag-pSi starting from 5×10^{-7} M concentration, yielding an EARE of 2×10^5. This finding could appear surprising because Raman mapping demonstrated a higher intensity of the SERS signal in the NIR range (this is true for any concentration at which 4-MBA can be detected, as shown in the inset of Figure 7c). However, the reason for such result can be found in the complexity of the polydisperse nanoparticle system. According to the hypothesis of the authors, which is supported by FESEM images analysis, Ag-pSi is characterized by the presence of a large number of interparticle gaps of the order of 20–30 nm

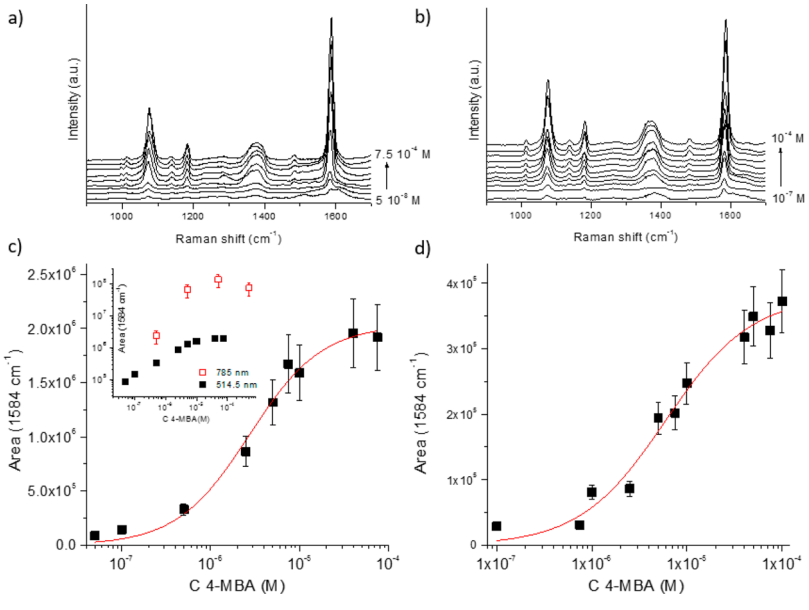

Figure 7. SERS spectra of 4-MBA at several concentrations (excitation at 514.5 nm) on (a) Ag-pSi and (b) Ag-PDMS. The corresponding Langmuir fits of the area of the 1584 cm^{-1} peak vs 4-MBA concentration are collected in (c) and (d), respectively. In the inset, peak areas calculated for Ag-pSi excited at 514.5 and 785 nm are compared.

and relatively few gaps lower than 10 nm. As pointed out by FEM simulations, intense resonances at wavelengths larger than 700 nm arise when the interparticle gap size is a few nanometers (for particle diameter of 100 nm, which is the average size in the Ag-pSi substrates). Therefore, nanoparticles that resonate with a 785 nm excitation are a small fraction only of the total population. When samples are incubated at 4-MBA concentrations as low as 10^{-8}–10^{-7} M, the density of molecules attached to the silver surface is extremely low, and the probability to have molecular adsorption in the nanometric gaps of facing NPs irradiated by the laser spot can be really small or even null. Thus, despite the huge enhancement potentially produced by the hot-spots hosted in the smallest interparticle gap, the scattering system cannot yield a detectable SERS signal. On the other hand, if Ag-pSi is excited at 514.5 nm, the density of the resonant scatterers is much higher than at 785 nm, even if the contribution to the overall enhancement of each interparticle junction is lower, thus providing a detectable SERS signal also at lower analyte concentration. For 4-MBA high concentration regimes, the adsorption of the analytes can occur also in several nanosized interparticle gaps, and in this case the higher amplification efficiency of these nanostructures makes the 4-MBA SERS intensity, for excitation at 785 nm, overwhelming in comparison with the intensity obtained for excitation at 514.5 nm.

The obtained results are comparable to other recently reported SERS substrates in terms of enhancement efficiency. Actually, 4-MBA adsorbed on nanoengineered silver dimers showed EF between 4.3×10^6 and 6.6×10^5,[38] while mesostructured gold NPs decorated cylinder micellas exhibited an EF of 10^6 in optimized conditions.[39] Self-assembled silver nanostructures provided a 3.87×10^5 to 1.99×10^6 enhancement for different particle shapes,[40] and a 2.8×10^6 EF was estimated for deposited silver nanotriangles.[41] Similar EF have been reported for several electronic off-resonant analytes.[42]

Finally, it is worth noting that the data can be fitted with a Langmuir isotherm over three concentration decades with good R^2 values (0.955 76 for Ag-pSi and 0.978 65 for Ag-PDMS), as shown in Figures 7c,d (except for 785 nm excitation of 4-MBA incubated on Ag-pSi, where the SERS intensities are affected by a noticeable fluctuation). This model can be applied when the system deals with a chemisorption equilibrium phenomenon in which the surface is characterized by a fixed number of binding sites. A threshold of around 5×10^{-5} M can be considered a high concentration regime where the SERS intensity approaches a saturation due to the formation of a monolayer and the depletion of adsorption sites.

Taking into account the Langmuir-like patterns evidenced in Figure 7, which can be considered reliable calibration curves, and the low standard deviation of the SERS signal obtained both for intrasample and intersamples measurements for Ag-PDMS, this substrate can be considered a substrate of choice to be employed in quantitative analysis.

CONCLUSIONS

Multiwavelength SERS analysis of Ag-coated PDMS and pSi substrates are performed in terms of enhancement efficiency and signal uniformity (i.e., repeatability). The experimental results and the modeling reveal that despite the high SERS intensity obtained for analytes incubated on Ag-pSi substrates (especially for excitation in the NIR range), a very high inhomogeneity limits their use in qualitative measurements. Conversely, Ag-PDMS substrates, which still provide a relevant SERS enhancement ($\sim 10^6$), show a much lower standard deviation both within the same substrate and when several substrates, synthesized under the same growth conditions, are compared (RSD ~ 10% and 20%, respectively). Moreover, the monotonic trend of the SERS signal intensity over 3 orders of magnitude of the analyte concentration demonstrates that Ag-PDMS substrates could be considered for quantitative SERS applications.

ASSOCIATED CONTENT

Supporting Information

The Supporting Information is available free of charge on the ACS Publications website at DOI: 10.1021/acs.jpcc.6b03852.

FESEM micrograph of as-prepared porous silicon, cross-sectional FESEM micrograph of Ag-pSi, and Ag-PDMS, EM near-field intensity distribution around a hemispheres dimer for the two substrates, extended SERS spectrum of 4-MBA and bands assignments, SERS intensity histograms at the three wavelengths extracted by the Raman maps, detailed calculation of the EARE (PDF)

AUTHOR INFORMATION

Corresponding Authors

*E-mail chiara.novara@polito.it; Tel +39-011-0904713 (C.N.).
*E-mail fabrizio.giorgis@polito.it; Tel +39-011-5647354 (F.G.).

Author Contributions

C.N. and S.D.M. contributed equally to this work.

Notes

The authors declare no competing financial interest.

ACKNOWLEDGMENTS

Financial support from Projects NANOMAX (Progetto Bandiera MIUR PNR (2011–2013) and NEWTON (MIUR FIRB 2011–2014) is gratefully acknowledged.

REFERENCES

(1) Banholzer, M. J.; Millstone, J. E.; Qin, L.; Mirkin, C. A. Rationally Designed Nanostructures for Surface-Enhanced Raman Spectroscopy. *Chem. Soc. Rev.* **2008**, *37*, 885–897.

(2) Stiles, P. L.; Dieringer, J. A.; Shah, N. C.; Van Duyne, R. P. Surface-Enhanced Raman Spectroscopy. *Annu. Rev. Anal. Chem.* **2008**, *1*, 601–626.

(3) Urban, A. S.; Shen, X.; Wang, Y.; Large, N.; Wang, H.; Knight, M. W.; Nordlander, P.; Chen, H.; Halas, N. J. Three-Dimensional Plasmonic Nanoclusters. *Nano Lett.* **2013**, *13*, 4399–4403.

(4) Lombardi, J. R.; Birke, R. L. Theory of Surface-Enhanced Raman Scattering in Semiconductors. *J. Phys. Chem. C* **2014**, *118*, 11120–11130.

(5) Lamberti, A.; Virga, A.; Chiadò, A.; Chiodoni, A.; Bejtka, K.; Rivolo, P.; Giorgis, F. Ultrasensitive Ag-Coated TiO 2 Nanotube Arrays for Flexible SERS-Based Optofluidic Devices. *J. Mater. Chem. C* **2015**, *3* (26), 6868–6875.

(6) Lamberti, A.; Virga, A.; Angelini, A.; Ricci, A.; Descrovi, E.; Cocuzza, M.; Giorgis, F. Metal–elastomer Nanostructures for Tunable SERS and Easy Microfluidic Integration. *RSC Adv.* **2015**, *5* (6), 4404–4410.

(7) Chan, S.; Kwon, S.; Koo, T.-W.; Lee, L. P.; Berlin, a. A. Surface-Enhanced Raman Scattering of Small Molecules from Silver-Coated Silicon Nanopores. *Adv. Mater.* **2003**, *15* (19), 1595–1598.

(8) Fan, M.; Andrade, G. F. S.; Brolo, A. G. A Review on the Fabrication of Substrates for Surface Enhanced Raman Spectroscopy

and Their Applications in Analytical Chemistry. *Anal. Chim. Acta* **2011**, *693* (1–2), 7–25.
(9) Bianco, G. V.; Losurdo, M.; Giangregorio, M. M.; Capezzuto, P.; Bruno, G. Direct Fabrication Route to Plastic-Supported Gold Nanoparticles for Flexible NIR-SERS. *Plasmonics* **2013**, *8* (1), 159–165.
(10) Yan, J.; Han, X.; He, J.; Kang, L.; Zhang, B.; Du, Y.; Zhao, H.; Dong, C.; Wang, H. L.; Xu, P. Highly Sensitive Surface-Enhanced Raman Spectroscopy (SERS) Platforms Based on Silver Nanostructures Fabricated on Polyaniline Membrane Surfaces. *ACS Appl. Mater. Interfaces* **2012**, *4* (5), 2752–2756.
(11) Lin, H.; Mock, J.; Smith, D.; Gao, T.; Sailor, M. J. Surface-Enhanced Raman Scattering from Silver-Plated Porous Silicon. *J. Phys. Chem. B* **2004**, *108*, 11654–11659.
(12) Giorgis, F.; Descrovi, E.; Chiodoni, A.; Froner, E.; Scarpa, M.; Venturello, A.; Geobaldo, F. Porous Silicon as Efficient Surface Enhanced Raman Scattering (SERS) Substrate. *Appl. Surf. Sci.* **2008**, *254* (22), 7494–7497.
(13) Virga, A.; Rivolo, P.; Frascella, F.; Angelini, A.; Descrovi, E.; Geobaldo, F.; Giorgis, F. Silver Nanoparticles on Porous Silicon: Approaching Single Molecule Detection in Resonant SERS Regime. *J. Phys. Chem. C* **2013**, *117* (39), 20139–20145.
(14) Shen, W.; Lin, X.; Jiang, C.; Li, C.; Lin, H.; Huang, J.; Wang, S.; Liu, G.; Yan, X.; Zhong, Q.; et al. Reliable Quantitative SERS Analysis Facilitated by Core-Shell Nanoparticles with Embedded Internal Standards. *Angew. Chem., Int. Ed.* **2015**, *54* (25), 7308–7312.
(15) Sun, L.; Irudayaraj, J. Quantitative Surface-Enhanced Raman for Gene Expression Estimation. *Biophys. J.* **2009**, *96* (11), 4709–4716.
(16) Bandarenka, H.; Artsemyeva, K.; Redko, S.; Panarin, A.; Terekhov, S.; Bondarenko, V. Effect of Swirl-like Resistivity Striations in N^+-Type Sb Doped Si Wafers on the Properties of Ag/porous Silicon SERS Substrates. *Phys. Status Solidi* **2013**, *10* (4), 624–627.
(17) Liu, Z.; Cheng, L.; Zhang, L.; Jing, C.; Shi, X.; Yang, Z. Nanoscale Large-Area Fabrication of Highly Reproducible Surface Enhanced Raman Substrate via a Facile Double Sided Tape-Assisted Transfer Approach. *Nanoscale* **2014**, *6*, 2567–2572.
(18) Wu, L.; Shen, B. Large-Scale Gold Nanoparticle Superlattice and Its SERS Properties for the Quantitative Detection of Toxic Carbaryl. *Nanoscale* **2013**, *5*, 5274–5278.
(19) Yang, Q.; Deng, M.; Li, H.; Li, M.; Zhang, C.; Shen, W.; Li, Y.; Guo, D.; Song, Y. Highly Reproducible SERS Arrays Directly Written by Inkjet Printing. *Nanoscale* **2015**, *7* (2), 421–425.
(20) Beleites, C.; Sergo, V. (2015): "hyperSpec: A Package to Handle Hyperspectral Data Sets in R". R package version 0.98-20150304; http://hyperspec.r-forge.r-project.org.
(21) R Core Team (2016): *A language and environment for statistical computing*; R Foundation for Statistical Computing: Vienna, Austria; URL https://www.R-project.org/.
(22) Harraz, F. A.; Tsuboi, T.; Sasano, J.; Sakka, T.; Ogata, Y. H. Metal Deposition onto a Porous Silicon Layer by Immersion Plating from Aqueous and Nonaqueous Solutions. *J. Electrochem. Soc.* **2002**, *149* (9), C456.
(23) Le Ru, E. C.; Etchegoin, P. G. Phenomenological Local Field Enhancement Factor Distributions around Electromagnetic Hot Spots. *J. Chem. Phys.* **2009**, *130* (18), 181101.
(24) Haynes, C. L.; Van Duyne, R. P. Plasmon-Sampled Surface-Enhanced Raman Excitation Spectroscopy. *J. Phys. Chem. B* **2003**, *107*, 7426–7433.
(25) Santoro, G.; Yu, S.; Schwartzkopf, M.; Zhang, P.; Koyiloth Vayalil, S.; Risch, J. F. H.; Rübhausen, M. A.; Hernández, M.; Domingo, C.; Roth, S. V. Silver Substrates for Surface Enhanced Raman Scattering: Correlation between Nanostructure and Raman Scattering Enhancement. *Appl. Phys. Lett.* **2014**, *104*, 243107.
(26) Virga, A.; Gazia, R.; Pallavidino, L.; Mandracci, P.; Descrovi, E.; Chiodoni, A.; Geobaldo, F.; Giorgis, F. Metal-Dielectric Nanostructures for Amplified Raman and Fluorescence Spectroscopy. *Phys. Status Solidi C* **2010**, *7* (3–4), 1196–1199.
(27) Xu, H.; Käll, M. Modeling the Optical Response of Nanoparticle-Based Surface Plasmon Resonance Sensors. *Sens. Actuators, B* **2002**, *87*, 244–249.
(28) Campaigne, E.; Meyer, W. W. Preparation and Absorption Spectra of P-Mercaptocinnamic and P-Mercaptobenzoic Acids and Derivatives. *J. Org. Chem.* **1962**, *27*, 2835.
(29) Michota, A.; Bukowska, J. Surface-Enhanced Raman Scattering (SERS) of 4-Mercaptobenzoic Acid on Silver and Gold Substrates. *J. Raman Spectrosc.* **2003**, *34* (1), 21–25.
(30) Herzog, J. B.; Knight, M. W.; Li, Y.; Evans, K. M.; Halas, N. J.; Natelson, D. Dark Plasmons in Hot Spot Generation and Polarization in Interelectrode Nanoscale Junctions. *Nano Lett.* **2013**, *13*, 1359–1364.
(31) Ahmadivand, A.; Pala, N.; Güney, D. Ö. Enhancement of Photothermal Heat Generation by Metallodielectric Nanoplasmonic Clusters. *Opt. Express* **2015**, *23* (11), 682–691.
(32) Hastings, S. P.; Swanglap, P.; Qian, Z.; Fang, Y.; Park, S.-J.; Link, S.; Engheta, N.; Fakhraai, Z. Quadrupole-Enhanced Raman Scattering. *ACS Nano* **2014**, *8* (9), 9025–9034.
(33) Theiss, J.; Aykol, M.; Pavaskar, P.; Cronin, S. B. Plasmonic Mode Mixing in Nanoparticle Dimers with Nm-Separations via Substrate-Mediated Coupling. *Nano Res.* **2014**, *7* (9), 1344–1354.
(34) Knight, M. W.; Wu, Y.; Lassiter, J. B.; Nordlander, P.; Halas, N. J. Substrates Matter: Influence of an Adjacent Dielectric on an Individual Plasmonic Nanoparticle 2009. *Nano Lett.* **2009**, *9* (5), 2188–2192.
(35) Radziuk, D.; Moehwald, H. Prospects for Plasmonic Hot Spots in Single Molecule SERS towards the Chemical Imaging of Live Cells. *Phys. Chem. Chem. Phys.* **2015**, *17* (33), 21072–21093.
(36) Camden, J. P.; Dieringer, J. A.; Wang, Y.; Masiello, D. J.; Marks, L. D.; Schatz, G. C.; Van Duyne, R. P. Probing the Structure of Single-Molecule Surface-Enhanced Raman Scattering Hot Spots. *J. Am. Chem. Soc.* **2008**, *130* (38), 12616–12617.
(37) Virga, A.; Rivolo, P.; Descrovi, E.; Chiolerio, A.; Digregorio, G.; Frascella, F.; Soster, M.; Bussolino, F.; Marchiò, S.; Geobaldo, F.; et al. SERS Active Ag Nanoparticles in Mesoporous Silicon: Detection of Organic Molecules and Peptide-Antibody Assays. *J. Raman Spectrosc.* **2012**, *43* (6), 730–736.
(38) Xia, X.; Li, W.; Zhang, Y.; Xia, Y. Silica-Coated Dimers of Silver Nanospheres as Surface-Enhanced Raman Scattering Tags for Imaging Cancer Cells. *Interface Focus* **2013**, *3* (3), 20120092.
(39) Lai, Y. H.; Chen, S. W.; Hayashi, M.; Shiu, Y. J.; Huang, C. C.; Chuang, W. T.; Su, C. J.; Jeng, H. C.; Chang, J. W.; Lee, Y. C.; et al. Mesostructured Arrays of Nanometer-Spaced Gold Nanoparticles for Ultrahigh Number Density of SERS Hot Spots. *Adv. Funct. Mater.* **2014**, *24* (17), 2544–2552.
(40) Zhu, S.; Fan, C.; Wang, J.; He, J.; Liang, E. Surface-Enhanced Raman Scattering of 4-Mercaptobenzoic Acid and Hemoglobin Adsorbed on Self-Assembled Ag Monolayer Films with Different Shapes. *Appl. Phys. A: Mater. Sci. Process.* **2014**, *117* (3), 1075–1083.
(41) Geng, X.; Leng, W.; Carter, N. A.; Vikesland, P. J.; Grove, T. Z. Protein-Aided Formation of Triangular Silver Nanoprisms with Enhanced SERS Performance. *J. Mater. Chem. B* **2016**, *4* (23), 4182–4190.
(42) Hoppmann, E. P.; Yu, W. W.; White, I. M. Highly Sensitive and Flexible Inkjet Printed SERS Sensors on Paper. *Methods* **2013**, *63*, 219–224.